



A single step unique microstructural growth of porous colossal dielectric constant titanium oxide

Sunil Meti¹ · Sagar Prutvi Hosangadi² · M. R. Rahman¹ · Udaya K. Bhat¹

Received: 3 December 2018 / Accepted: 4 February 2019 / Published online: 18 February 2019
© Springer-Verlag GmbH Germany, part of Springer Nature 2019

Abstract

New microstructure of TiO_2 grown in hydrothermal process is reported on. The influence of hydrothermal process parameters, such as heating temperature, on growth dynamics is also reported. The improvement in surface area and crystallinity are reached by the hydrothermal process, as compared to other growth techniques. The synthesized TiO_2 is characterized by XRD technique and subjected to Rietveld analysis. The results indicate that the obtained TiO_2 is of tetragonal structure. The results of other characterization techniques such as micrography, Raman spectroscopy and TGA are also reported. The obtained TiO_2 is tested for its electrical properties and it shows good dielectric strength in the flat band region from 40 Hz to 1 MHz.

1 Introduction

The human race for its comforts is concentrating on automation of all the equipment and processes. The drive of automation has made engineers to implement sensors in most of the machineries, creating the Internet of things (IoT) network. As the IoT network is growing rapidly, the requirement of better batteries and capacitors is also gaining importance. The present energy storage devices have various limitations such as chemical leaching, and e-waste disposal. There is a need for finding out better energy storage materials as a replacement. It is found that the nanomaterials could replace the present energy storing devices due to their unique advantages [1]. The materials at nanoscale behave differently compared to their bulk state. The nanomaterials have a higher surface to volume ratio compared to the bulk counterpart, and thus increasing energy storage capability. The surface atoms present in such nanomaterials are known to be highly active and makes a significant contribution to the total free energy [2].

Presently, the batteries fulfill the role of storing energy. To overcome the limitations of the batteries such as transportation, ageing, cost, and protection from being over charged and discharged, capacitors are proposed as future energy storage devices. It is easy to use and requires less time for charging the capacitors, as compared to batteries. The charge storage capacity of the capacitor depends on the dielectric material. There are various dielectric materials reported, such as TiO_2 , BaTiO_3 , $\text{CaCu}_3\text{Ti}_4\text{O}_{12}$, La_2O_3 , and Al_2O_3 [3–8]. Amongst, TiO_2 is one of the most abundant compound and a very useful material for a variety of applications [9–12]. TiO_2 possess unique physical and chemical characteristics with abundance in availability and nontoxicity, as well as high thermal and chemical stability [13]. TiO_2 is used in such areas as gas sensors, biomedical implants, self-cleaning glasses, dye-sensitized solar cells, cosmetics and photocatalytic applications [14–18]. Besides, TiO_2 is actively used in integrated optics and electronics [19–22]. TiO_2 possess three different crystalline modifications, namely, anatase, rutile and brookite [18, 23]. There are varieties of TiO_2 synthesis techniques reported, namely, sol-gel, combustion synthesis, sputtering, hydrothermal synthesis, etc. [10, 24–26]; amongst these, the hydrothermal synthesis technique has unique advantages such as uniform crystal growth, less instrumentation, rapid and easy method [23, 27]. In the hydrothermal method, the morphology, microstructure and phase composition of TiO_2 could be easily altered by varying the process parameters [27]. Different morphologies of the TiO_2 and their properties are reviewed

✉ Udaya K. Bhat
udayabhatk@gmail.com

¹ Department of Metallurgical and Materials Engineering,
National Institute of Technology Karnataka,
Surathkal 575025, India

² Department of Metallurgical Engineering and Material
Science, Indian Institute of Technology Bombay, Powai,
Mumbai 400076, India

in the literature [23]. The TiO_2 material is already been tested as a superior dielectric material [28–31].

In this work, TiO_2 with a unique porous morphology is successfully synthesized via hydrothermal method. The material is characterized to confirm the morphology and phase composition. The effect of hydrothermal heating temperature on the microstructural or morphological growth of the TiO_2 is also examined. The dielectric behaviour of the TiO_2 film has been examined in flat band regime ranging from 40 Hz to 1 MHz. The AC conductivity study is also implemented to know the electrical property of the material.

2 Materials and synthesis methods

2.1 Materials

All the chemicals were commercially available and were used without further purification.

2.2 Synthesis

0.5 g of ammonium hexafluorotitanate ($(\text{NH}_4)_2\text{TiF}_6$ – with purity 99.99%, Sigma Aldrich) is added into 40 ml of deionised water. 20 ml of diethanolamine (Sigma Aldrich) is added gently under constant stirring for 30 min. The colour of the solution turns to brown. Then, the solution is transferred into a Teflon-lined stainless steel autoclave. Fluorine-Tin-Oxide coated (FTO, Sigma Aldrich) glass slides (dimensions: $10 \times 2.5 \times 0.5$ cm) having a sheet resistance of 12–15 Ω per square are kept inside the autoclave to get the TiO_2 film deposited on the glass slides. The autoclave is heated in a hot air oven for 24 h at different temperatures, i.e., 120 °C (called as sample T), 150 °C (called as sample T1) and 180 °C (called as sample T2). The sample “T (120 °C)” has not yielded any morphology and is discussed in the supplementary information section (S1). The autoclave is removed from the oven and is naturally allowed to cool down to room temperature. The deposited glass slides are collected and washed with absolute alcohol and DI water several times. Finally, the glass slides are dried at 60 °C for 12 h [27].

2.3 Characterization

The X-ray diffraction patterns were obtained (XRD, machine-Rigaku, Japan) with Cu-K α radiation ($\lambda = 1.5406$ Å) in the 2θ range from 5° to 80°. The scanning speed of XRD was 2°/min with 0.02° step. General Structural Analysis System (GSAS) software suite was used for the Rietveld method for the obtained XRD patterns [32–34]. SEM with an energy dispersive spectroscopy (SEM, machine-JEOL-JSM-6380LA, EDS from Oxford Instruments) was used to examine the morphology and the

elemental composition of the samples. The band energy was studied at room temperature using Raman spectroscopy (Raman, machine-Horiba Jobin Yvon - LabRAM HR spectrometer). The wavelengths of the laser source used were 325 and 514 nm. The TGA was carried out using (Thermo-gravimetric Analyzer; PerkinElmer, TGA 4000) over the temperature range of 50–800 °C using a 20°C/min step. The specific surface area measurement was done using a Brunauer-Emmett-Teller (BET) apparatus under the standard protocols at 77 K. The TiO_2 sample was degassed under flowing N_2 at 300 °C overnight prior to BET measurements [35]. The chemical state of elements present in the TiO_2 was interrogated using X-ray photoelectron spectroscopy (XPS; PHI5000VersaProbeII) with Al – K α radiation (~1486.6 eV). All XPS data were calibrated with the C 1 s peak assigned at 284.7 eV. The deconvolution of O 1 s spectra was done using Gaussian–Lorentzian peak function after doing Shirley background subtraction. Impedance spectrometer (IM3536, Hioki, Japan) was used for the dielectric measurement. The dielectric constant, loss and conductivity studies were done at a frequency in the range from 40 Hz to 1 MHz. The details of the electrode parameters and dielectric properties measurement of as deposited TiO_2 film is explained with schematic diagram in supplementary section (S1).

3 Results and discussion

3.1 XRD analysis of the TiO_2 film

In Fig. 1a, the XRD spectra of samples T1 and T2 are shown. The peaks of samples T1 and T2 are perfectly attributed to the anatase phase (JCPDS card no. 21-1272) [11, 36]. The presence of diffraction peak (004) suggests the dominant crystal growth of TiO_2 along [001] direction [13, 16], which is typical for anatase TiO_2 nanoparticles. The absence of peaks belonging to impurities suggests the presence of pure anatase TiO_2 phase. The hydrothermal synthesis of TiO_2 affects the purity by the elimination of the surfactant. It results in the formation of pure mesoporous structure [37]. The strong and broad peaks indicate that the material has good crystallinity with small crystallite size. The crystallite size of the TiO_2 samples have been estimated from the full-width at half-maximum β (in radian) of the main peak (101) using the Scherrer equation [38]:

$$\tau = \frac{K\lambda}{\beta \cos \theta}$$

where τ is the crystallite size, θ is the diffraction angle, λ is 1.54 Å for the Cu K α line and K is the Scherrer constant. The value of K depends on the crystal shape and diffraction

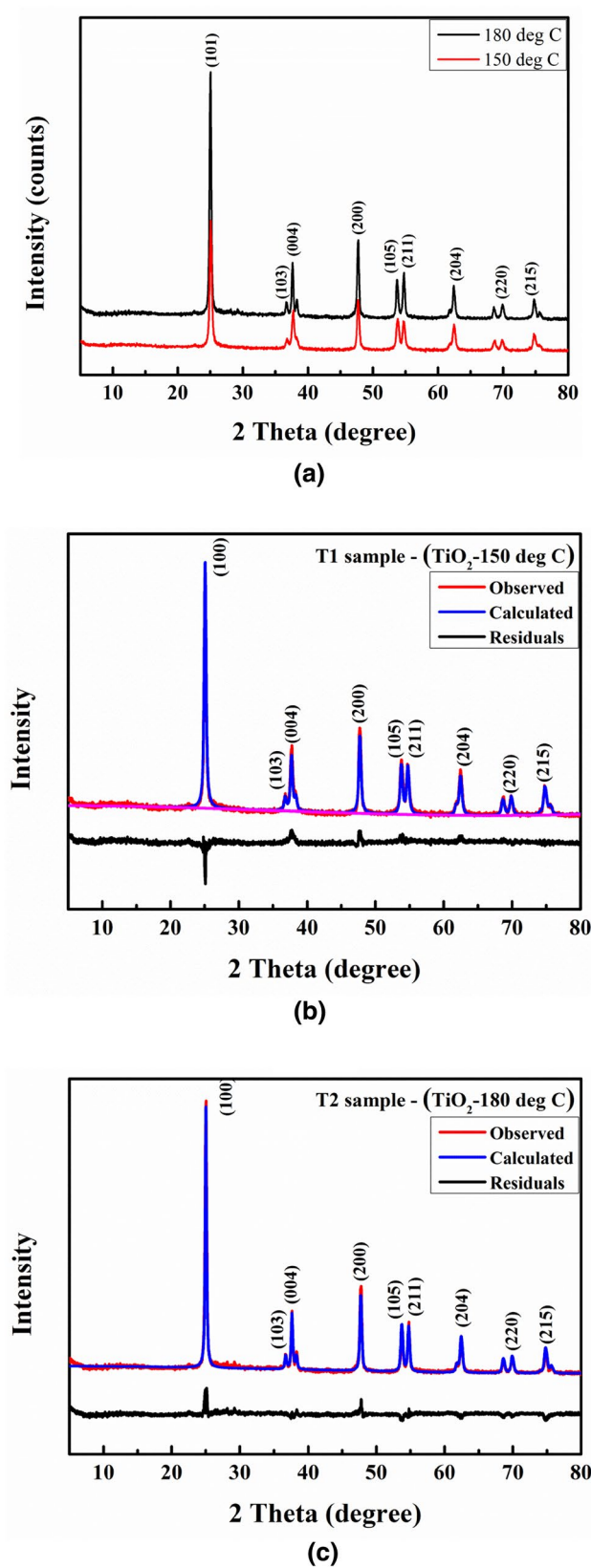


Fig. 1 **a** XRD spectra of TiO_2 samples T1 ($150\text{ }^\circ\text{C}$) and T2 ($180\text{ }^\circ\text{C}$) and corresponding Rietveld refined pattern of **b** T1 sample (synthesized at $150\text{ }^\circ\text{C}$) and **c** T2 sample (synthesized at $180\text{ }^\circ\text{C}$), respectively

Table 1 The refined parameters and crystal data of T1 and T2 TiO_2 samples

Parameters	Results	
	Sample T1 ($150\text{ }^\circ\text{C}$)	Sample T2 ($180\text{ }^\circ\text{C}$)
Crystal structure	Tetragonal	Tetragonal
Space group	$I4_1/\text{amd}$	$I4_1/\text{amd}$
$a\text{ \AA}$	3.7986	3.7940
$b\text{ \AA}$	3.7986	3.7940
$c\text{ \AA}$	9.499	9.5016
$\alpha\text{ (}^\circ\text{)}$	90	90
$\beta\text{ (}^\circ\text{)}$	90	90
$\gamma\text{ (}^\circ\text{)}$	90	90
R_p (profile factor)	8.82%	8.68%
R_{wp} (weighted profile factor)	10.96%	10.92%
Cell volume	137.068	136.775
χ^2	1.641	2.066

line indices [39]. The calculated crystallite size in the TiO_2 samples T1 and T2 are found out to be 22.6 nm and 20.3 nm, respectively. The increase in heating temperature decreases the crystallite size for sample T2 compared to T1. The diffraction peaks of sample T2 are sharper than these of the sample T1. This indicates that the sample T2 has better crystallization and smaller crystallites. It is attributed to exposure of the sample to the higher heating temperature [12].

The TiO_2 XRD data are further analyzed employing Rietveld refinement technique with the help of GSAS software, as shown in Fig. 1b, c [40]. The TiO_2 samples are found to crystallize in single anatase tetragonal structure with space group $I4_1/\text{amd}$ (JCPDS card no. 21-1272) without any other phase. In Fig. 1b, c, the experimental pattern (observed) is shown by red colour and theoretical data (calculated) are shown as blue colour. The difference between theoretical and experimental data is shown by black curve. The main refined parameters, crystal system, cell parameters (a, b, c) and atomic position (x, y, z) are presented in Table 1. The value of χ^2 for sample T1 and T2 is found out to be equal to 1.64 and 2.06, respectively. The lattice parameters obtained are in good agreement with the literature (JCPDS card no. 21-1272).

3.2 SEM analysis of the TiO_2 film

SEM micrographs of the T1 and T2 samples are shown in Fig. 2. The micrographs show that the sample T1 has the flower morphology and T2 sample has a flower-like morphology with higher dimension than that of sample T1. This TiO_2 crystals grow predominantly in [001] direction, as indicated by XRD results.

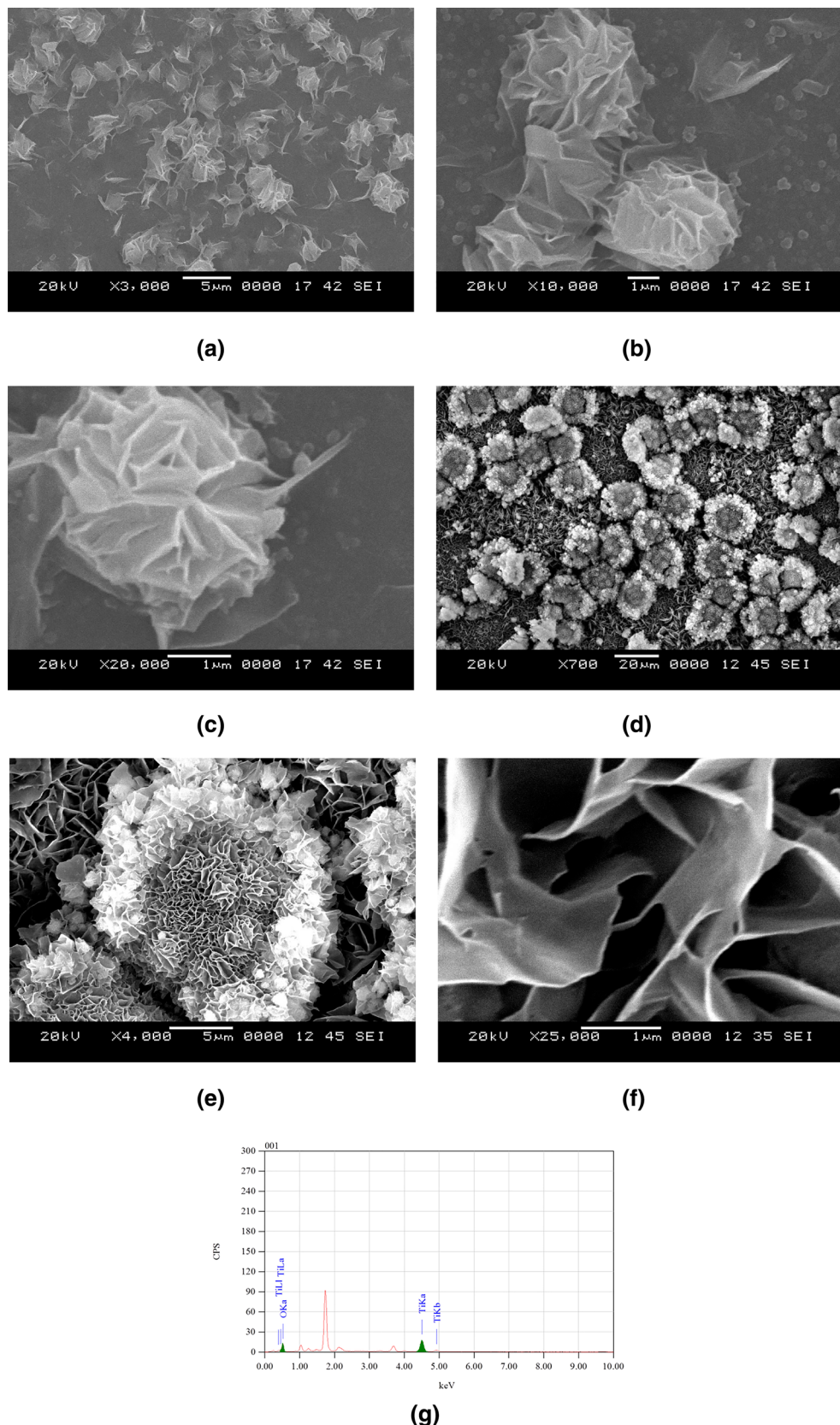


Fig. 2 SEM micrographs of porous flower-like TiO_2 microstructure for samples at T1 (150°C) (a, b and c) and T2 (180°C) (d, e, and f) at different magnifications and g SEM-EDS of TiO_2 sample

To understand the growth mechanism of 3D hierarchical TiO_2 , we investigated the corresponding temperature-dependent evolution of morphology and crystal structure of the samples. Figure 2 shows the SEM micrographs of samples fabricated at different reaction temperatures for 24 h of heating. The sample obtained at 120 °C has not yielded any morphology due to the lower reaction temperature (Further details are discussed in S1). After hydrothermal heating at 150 °C (T1) for 24 h, the microspheres with an average diameter of 3.0 μm are formed (Fig. 2a). The high-resolution SEM micrographs (in Fig. 2b,c) further confirms that the microspheres have a cluster of petals morphology. After the hydrothermal reaction at 180 °C (T2) for 24 h, however, the morphology of the microspheres changes obviously. Not only the diameter of microspheres increased to 20–30 μm , but also the microsphere surface becomes dense. As shown in Fig. 2d, most of the microspheres start showing 3D flower-like morphology with dense petals of thin nano TiO_2 layers. The high-resolution images in Fig. 2e,f, show that each petal in flower-like morphology is having a thickness in nanometers. The size of each microsphere in the sample T2 is greater than that in T1 due to heating temperature increase. The increase in heating temperature resulted in higher mobility of Ti^{4+} and O^{2-} ions [41, 42]. The increase in temperature also resulted in higher porosity, increased surface area and the growth of highly crystalline TiO_2 layered flower morphology (T2 compared to T1). Figure 2g also shows the SEM-EDS spectra of TiO_2 flower-like morphology. It is found that Ti and O are the only elements present in the material. Fractions (atomic weight) of Ti and O in the TiO_2 are found to be 33.89% and 66.11%, respectively. The EDS results clearly verify the stoichiometric nature of the deposits.

3.3 Raman analysis of the TiO_2 film

The TiO_2 Raman spectra of T1 and T2 samples are shown in Fig. 3. The graph interprets the quantitative analysis of percentage growth of TiO_2 in {001} facets [12, 16]. The characteristic vibration modes of anatase TiO_2 are located at 143 cm^{-1} (E_g), 395 cm^{-1} (B_{1g}), 516 cm^{-1} (A_{1g}) and 635 cm^{-1} (E_g), being consistent with the XRD results [43, 44]. The percentage of {001} facets were calculated for both samples by measuring the peak intensity ratio of the E_g (at 143 cm^{-1}) and A_{1g} (at 514 cm^{-1}) [12]. The percentage of {001} facets for sample T1 and T2 is calculated as 25% and 61%, respectively. Raman analysis results show the growth of the {001} facet is predominant for the T2 sample synthesized at 180 °C.

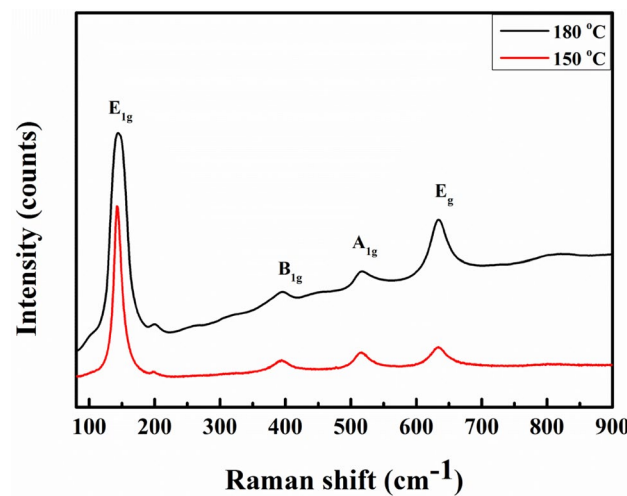


Fig. 3 Raman spectra showing characteristic bands of TiO_2 anatase phase for the samples T1 (150 °C) and T2 (180 °C)

3.4 XPS analysis

Figure 4 shows a survey and high-resolution XPS spectra of sample T2. The survey spectra showed that Ti and O are the only elements present in the sample. The C 1 s peak is present due to adsorbed hydrocarbons. In the XPS spectrum (Fig. 4b), the Ti 2p doublet has the components $\text{Ti } 2p_{3/2}$ (binding energy 456.8 eV) and $\text{Ti } 2p_{1/2}$ (binding energy 462.8) arise from spin-orbit splitting [45, 46]. The O 1 s spectrum of the sample T2 is deconvoluted with two peaks shown in Fig. 4c [43]. The components at binding energy 528 eV and 529.7 eV are attributed to lattice oxygen and -OH groups adsorbed on the surface of the TiO_2 , respectively [16, 47, 48].

3.5 TGA analysis of the TiO_2 film

In the TGA experiments, the samples T1 and T2 are heated from room temperature up to 800 °C in nitrogen atmosphere. The TGA curve shown in Fig. 5 reveals that the total weight losses for the samples T1 and T2 are 5.32% and 5.46%, respectively. The weight losses in the sample follow almost the same trend. There is a gradual weight loss occurring around 220 °C up to 680 °C due to surfactant decomposition [37]. The TiO_2 samples have a stable phase (anatase) after 680 °C, due to which the weight loss is negligible. According to the nitrogen (N_2) absorption and desorption graph, the specific surface area calculated by the Brunauer-Emmett-Teller (BET) equation from the data is $172.56 \text{ m}^2/\text{g}$ which is predominant compared to already published results [12, 24, 27]. The higher surface area is useful for the charge polarization which results in increased dielectric strength.

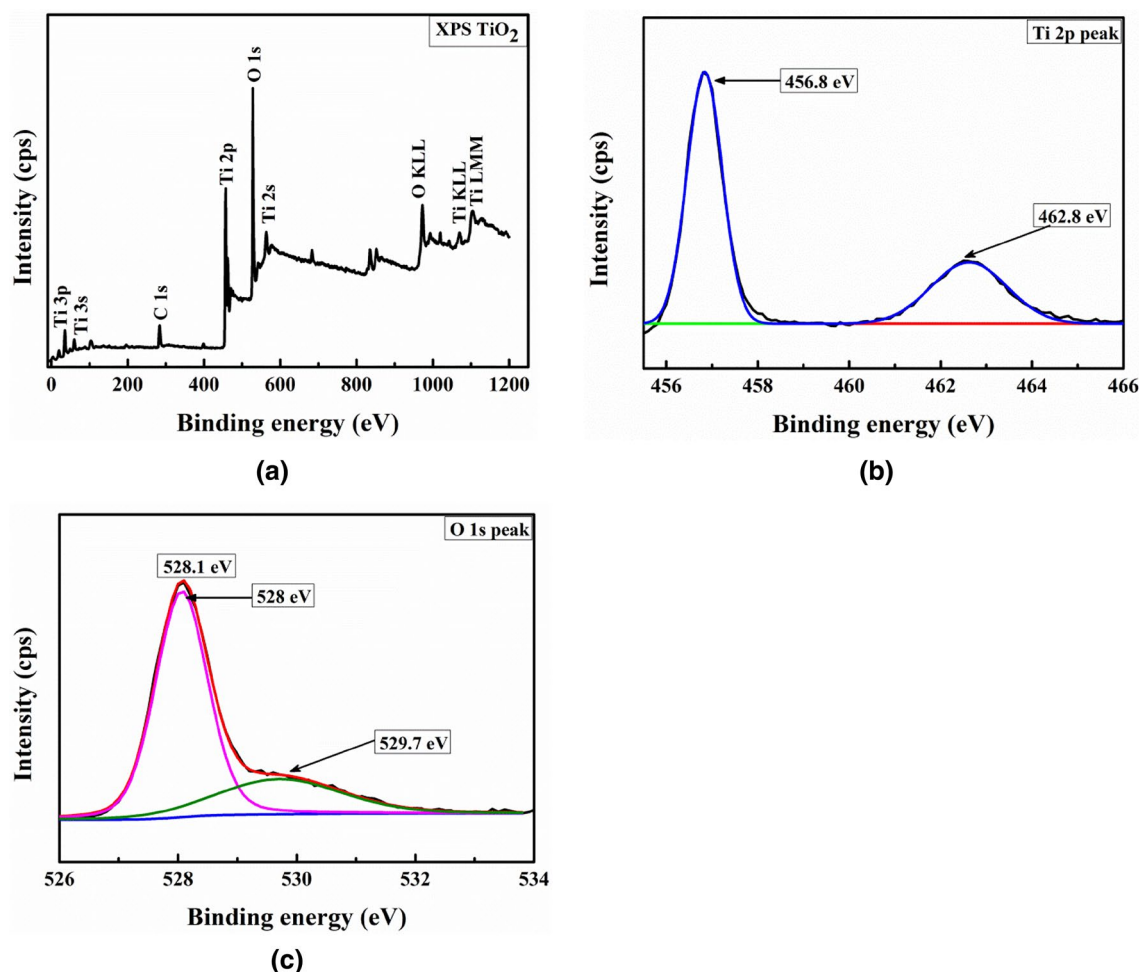


Fig. 4 **a** The XPS survey spectrum of the TiO_2 sample, **b** core level 2p spectrum of titanium and **c** core level 1 s spectrum of oxygen

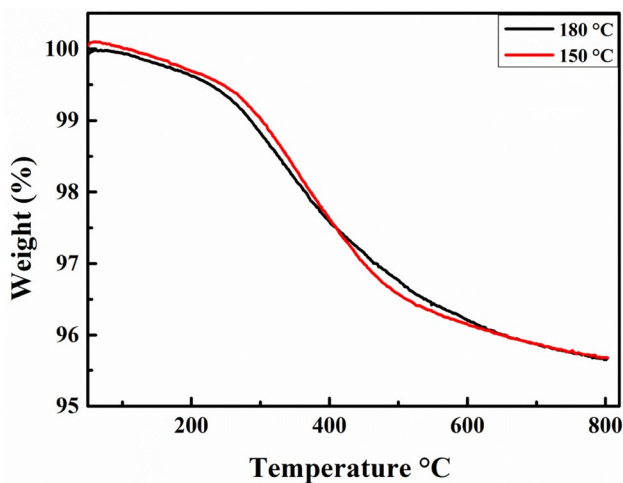


Fig. 5 The TGA graph T1 and T2 TiO_2 samples

3.6 Dielectric studies

The dielectric constant and the dielectric loss for the samples T1 and T2 are studied as a function of frequency, as shown in Fig. 6. The dielectric permittivity is evaluated using the relation,

$$\epsilon(r) = \frac{Cd}{\epsilon_0 A}.$$

where d is the thickness of dielectric film and A is the sample area.

Figure 6a shows the variation of dielectric constant against frequency for the T1 and T2 samples. At lower frequencies, the dielectric constant is high and it decrements expeditiously with a small increment in frequency for both samples T1 and T2. The dielectric constant of sample T2 is higher, as compared to that of T1, due to the following reasons. The T2 sample compared to T1 has higher $\{001\}$ facet number, porosity, grain boundary and

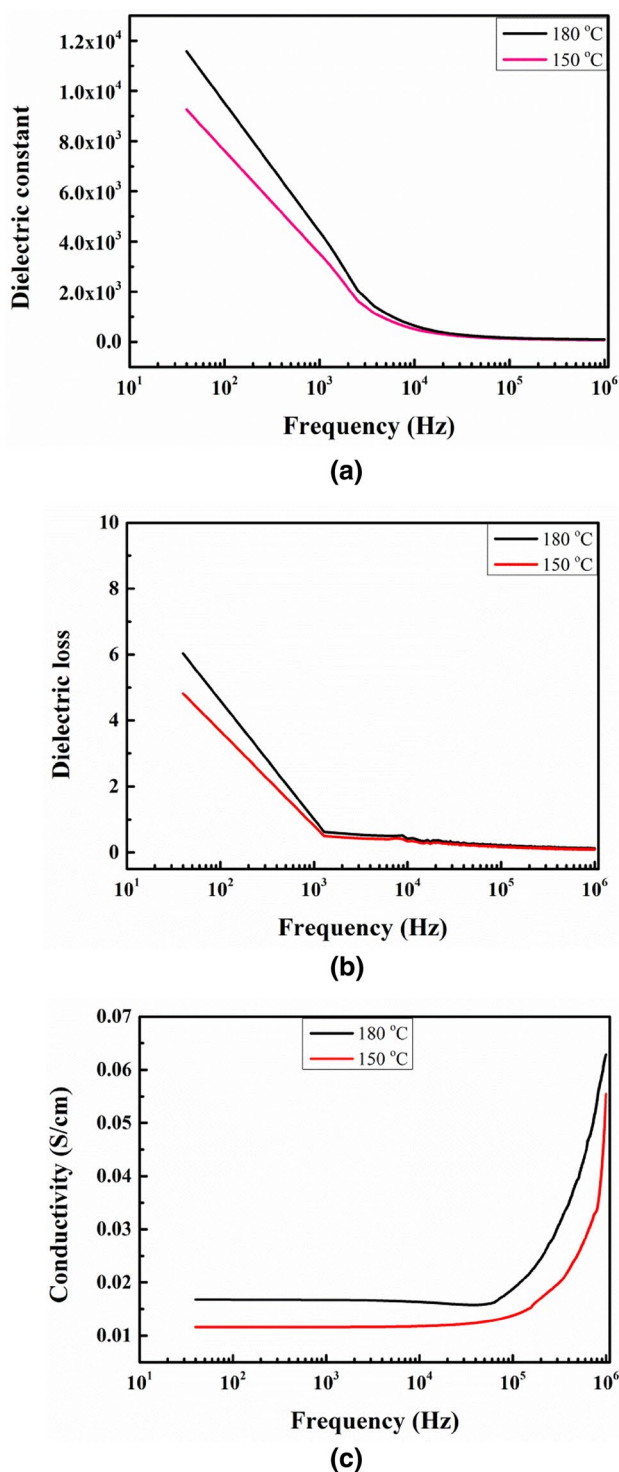


Fig. 6 The graphs of **a** The dielectric constant, **b** dielectric loss and **c** conductivity v/s frequency for the T1 and T2 TiO_2 samples

specific surface area. The increased space charge and ion jump orientation effect, observed in the porous flower-like morphology of the sample T2, results in a high value of dielectric constant compared to that of T1 [49]. The

sample T2 has higher number of grain boundaries than that of T1, where most of the electrical (electron–hole pairs) species are trapped. When voltage is applied, the large amount of charges are stored at the grain boundaries as a result of charge trapping. This phenomenon will affect the dielectric behaviour of the materials [50]. At lower frequencies, the dipole moment can facilely follow the transmutations in the electric field.

The dielectric constant of the T2 (flower-like) sample is higher than that of the T1 due to the increased rotational and space charge polarization effects [51]. These phenomenon occurs mainly in the interfaces and affects the dielectric constant [7, 52].

At 40 Hz, the dielectric permittivity is 11,571 and 9,256 for T2 and T1 samples, respectively. As the frequency increases, the dielectric permittivity decreases. The dielectric permittivity at 1 kHz was found out to be 3515 and 4473 for T1 and T2 samples, respectively. The value is superior to the already published reports [28]. Even at high frequencies, the TiO_2 retains a good dielectric strength.

At 1 MHz, the dielectric permittivity is found out to be 95 and 76 for T2 and T1 samples, respectively. As shown in Fig. 6b, the dielectric loss also decreases with increase in frequency for both the TiO_2 samples. The loss angle has almost the same value at higher frequencies [6]. The dielectric loss occurs due to the following reasons; the charge associated with the TiO_2 orient along the direction of the applied electric field. A part of the applied electric energy is utilized by the charge on the TiO_2 to overcome the internal friction forces [7]. Another small quantity of the applied electric energy is utilized for the rotation of charges from one position to another [53]. In nanophase TiO_2 materials, the dielectric loss occurs due to inhomogeneities (defects). The loss also occurs due to space charge formation at the interface layers which create an absorption current [54–56]. The dielectric loss calculated at 1 kHz is 0.78 and 1.02 for the T1 and T2 samples, respectively. Figure 6c shows the variation of conductivity with frequency. Initially, the conductivity is very low and it increases exponentially. The conductivity is high at higher frequency [54]. The conductivity for T1 and T2 samples at 1 kHz frequency calculated from the graph in Fig. 6c is 0.0108 S/cm and 0.0161 S/cm, respectively. This is due to the reason that the dielectric material loses its strength and makes the electric charge to flow through the material.

4 Conclusion

A novel single step facile hydrothermal route to synthesize porous flower-like TiO_2 material in the mixed solvents of diethanolamine and distilled water was presented. The BET results and SEM micrographs reveal that TiO_2 material

exhibited higher surface area. The XRD and Raman results showed that as-synthesized TiO_2 was highly crystalline and anatase in nature. The exposed high surface of the TiO_2 sample resulted in charge storage in terms of polarization effect. The effective surface utilized for charge storage was much higher in the flower-like morphology of TiO_2 T2 sample compared to T1. At 1 kHz, the dielectric permittivity (ϵ_r) for the TiO_2 samples synthesized at 180 °C (T2) and 150 °C (T1) were found to be 4473 and 3515, respectively. The conductivity study revealed that the conductivity increases with increase in frequency. At higher frequency, the TiO_2 becomes almost a good conductor due to the alignment of the polar molecules along the applied electric field. The TiO_2 flower-like morphology has features for the application as high dielectric strength material.

Acknowledgements Mr Sunil Meti is thankful to NITK, Surathkal, India and MHRD India for supporting the research in form of the Institute Research Fellowship. The Authors would like to acknowledge the Central Surface Analytical Facility of IIT Bombay for XPS studies. Authors also extend regards to Ms Rashmi for her assistance in SEM characterization.

References

- J. Jeevanandam, A. Barhoum, Y.S. Chan, A. Dufresne, M.K. Danquah, Review on nanoparticles and nanostructured materials: history, sources, toxicity and regulations. *Beilstein J. Nanotechnol.* **9**, 1050–1074 (2018). <https://doi.org/10.3762/bjnano.9.98>
- Z. Zhao, J. Tian, Y. Sang, A. Cabot, H. Liu, Structure, synthesis, and applications of TiO_2 nanobelts. *Adv. Mater.* **27**, 2557–2582 (2015). <https://doi.org/10.1002/adma.201405589>
- M. Dahl, Y. Liu, Y. Yin, Composite titanium dioxide nanomaterials nanomaterials. *Chem. Rev.* **114**, 9853–9889 (2014). <https://doi.org/10.1021/cr400634p>
- G. Wang, X. Huang, P. Jiang, Mussel-inspired fluoro-polydopamine functionalization of titanium dioxide nanowires for polymer nanocomposites with significantly enhanced energy storage capability. *Sci. Rep.* **7**, 1–12 (2017). <https://doi.org/10.1038/srep43071>
- C.A. Grabowski, S.P. Fillery, H. Koerner, M. Tchoul, L. Drummy, C.W. Beier, R.L. Brutchev, M.F. Durstock, R.A. Vaia, Dielectric performance of high permittivity nanocomposites: impact of polystyrene grafting on BaTiO_3 and TiO_2 . *Nanocomposites* **2** (2016) 117–124. <https://doi.org/10.1080/20550324.2016.1223913>
- B.V. Prasad, G.N. Rao, J.W. Chen, D. Suresh, Babu, Abnormal high dielectric constant in SmFeO_3 semiconductor ceramics. *Mater. Res. Bull.* **46**, 1670–1673 (2011). <https://doi.org/10.1016/j.materresbull.2011.06.001>
- A. Kumar, B.P. Singh, R.N.P. Choudhary, A.K. Thakur, Characterization of electrical properties of Pb-modified BaSnO_3 using impedance spectroscopy. *Mater. Chem. Phys.* **99**, 150–159 (2006). <https://doi.org/10.1016/J.MATCHEMPHYS.2005.09.086>
- B. Gupta, P. Pujar, S.S. Mal, D. Gupta, S. Mandal, Retention of high dielectric constant sodium beta alumina via solution combustion: Role of aluminum ions complexation with fuel. *Ceram. Int.* **44**, 1500–1511 (2018). <https://doi.org/10.1016/J.CERAMINT.2017.10.061>
- S. Xiong, Y. Tang, H.S. Ng, X. Zhao, Z. Jiang, Z. Chen, K.W. Ng, S. Chye, J. Loo, Specific surface area of titanium dioxide (TiO_2) particles influences cyto- and photo-toxicity. *Toxicology* **304** (2013) 132–140. <https://doi.org/10.1016/j.tox.2012.12.015>
- S. Meti, U.B. K, M.R. Rahman, M. Jayalakshmi, Photocatalytic behaviour of nanocomposites of sputtered titanium oxide film on graphene oxide nanosheets. *Am. J. Mater. Sci.* **5**, 12–18 (2015). <https://doi.org/10.5923/c.materials.201502.03>
- V. Štengl, S. Bakardjieva, T.M. Grygar, J. Bludská, M. Kormunda, TiO_2 -graphene oxide nanocomposite as advanced photocatalytic materials. *Chem. Cent. J.* **7**, 41 (2013). <https://doi.org/10.1186/1752-153X-7-41>
- L. Chu, Z. Qin, J. Yang, X. Li, Anatase TiO_2 nanoparticles with exposed {001} facets for efficient dye-sensitized solar cells. *Sci. Rep.* **5**, 12143 (2015). <https://doi.org/10.1038/srep12143>
- J. Tao, X. Dong, H. Zhu, H. Tao, P. He, Enhanced photocatalytic properties of ultra-long nanofiber synthesized from pure titanium powders. *Rare Met.* **31**, 39–42 (2012). <https://doi.org/10.1007/s12598-012-0459-x>
- J. Fan, Z. Li, W. Zhou, Y. Miao, Y. Zhang, J. Hu, G. Shao, Dye-sensitized solar cells based on TiO_2 nanoparticles/nanobelts double-layered film with improved photovoltaic performance. *Appl. Surf. Sci.* **319**, 75–82 (2014). <https://doi.org/10.1016/JAPSUS.C.2014.07.054>
- W.J. Lee, Y.M. Sung, Synthesis of anatase nanosheets with exposed (001) facets via chemical vapor deposition. *Cryst. Growth Des.* **12**, 5792–5795 (2012). <https://doi.org/10.1021/cg301317j>
- K.R.N. Pai, G.S. Anjusree, T.G. Deepak, D. Subash, S.V. Nair, A.S. Nair, High surface area TiO_2 nanoparticles by a freeze-drying approach for dye-sensitized solar cells. *RSC Adv.* **4**, 36821–36827 (2014). <https://doi.org/10.1039/C4RA04226C>
- M. Ben Yahia, F. Lemoigno, T. Beuvier, J. Filhol, M. Richard-Plouet, L. Brohan, M.L. Doublet, Updated references for the structural, electronic, and vibrational properties of TiO_2 (B) bulk using first-principles density functional theory calculations. *J. Chem. Phys.* **130** (2009). <https://doi.org/10.1063/1.3130674>
- J. Low, B. Cheng, J. Yu, Surface modification and enhanced photocatalytic CO 2 reduction performance of TiO_2 : a review. *Appl. Surf. Sci.* **392**, 658–686 (2017). <https://doi.org/10.1016/j.apsusc.2016.09.093>
- I.E. Kalabin, T.I. Grigorieva, L.D. Pokrovsky, D.V. Sheglov, D.I. Shevtsov, V.V. Atuchin, Nanofaceting of LiNbO_3 X-cut surface by high temperature annealing and titanium diffusion. *Opt. Commun.* **221**, 359–363 (2003). [https://doi.org/10.1016/S0030-4018\(03\)01537-2](https://doi.org/10.1016/S0030-4018(03)01537-2)
- V.V. Atuchin, T.I. Grigorieva, I.E. Kalabin, V.G. Kesler, L.D. Pokrovsky, D.I. Shevtsov, Comparative analysis of electronic structure of Ti:LiNbO_3 and LiNbO_3 surfaces. *J. Cryst. Growth* **275**, e1603–e1607 (2005). <https://doi.org/10.1016/J.JCRYSGRO.2004.11.176>
- Z. Hu, L. Zhao, H. Guo, S. Wang, W. Li, X. Yang, B. Dong, L. Wan, Novel double-layered photoanodes based on porous-hollow TiO_2 -microspheres and $\text{La}(\text{OH})_3\text{:Yb}_3^+/\text{Er}_3^+$ for highly efficient dye-sensitized solar cells, *J. Mater. Sci. Mater. Electron.* **1–9** (2018). <https://doi.org/10.1007/s10854-018-0283-7>
- V.V. Atuchin, M.S. Lebedev, I.V. Korolkov, V.N. Kruchinin, E.A. Maksimovskii, S.V. Trubin, Composition-sensitive growth kinetics and dispersive optical properties of thin $\text{Hf}_x\text{Ti}_{1-x}\text{O}_2$ ($0 \leq x \leq 1$) films prepared by the ALD method, *J. Mater. Sci. Mater. Electron.* **1–12** (2018). <https://doi.org/10.1007/s10854-018-0351-z>
- C.P. Sajan, S. Wageh, A.A. Al-Ghamdi, J. Yu, S. Cao, TiO_2 nanosheets with exposed {001} facets for photocatalytic applications. *Nano Res.* **9**, 3–27 (2016). <https://doi.org/10.1007/s12274-015-0919-3>
- F. Jin, H. Tong, L. Shen, K. Wang, P.K. Chu, Micro-structural and dielectric properties of porous TiO_2 films synthesized on titanium alloys by micro-arc discharge oxidation. *Mater. Chem. Phys.* **100**, 31–33 (2006). <https://doi.org/10.1016/j.matchemphys.s.2005.12.001>

25. I.B. Troitskaia, T.A. Gavrilova, V.V. Atuchin, Structure and micro-morphology of titanium dioxide nanoporous microspheres formed in water solution. *Phys. Procedia*. **23**, 65–68 (2012). <https://doi.org/10.1016/J.PHPR.2012.01.017>
26. V.N. Kruchinin, T.V. Perevalov, V.V. Atuchin, V.A. Gritsenko, A.I. Komonov, I.V. Korolkov, L.D. Pokrovsky, C.W. Shih, A. Chin, Optical properties of TiO_2 films deposited by reactive electron beam sputtering. *J. Electron. Mater.* **46**, 6089–6095 (2017). <https://doi.org/10.1007/s11664-017-5552-3>
27. G.E. Cheng, Y. Zhang, H.Z. Ke, T.T. Hao, Y.Z. Wang, Hydro-thermal synthesis of TiO_2 /reduced graphene oxide nanocomposite with enhanced photocatalytic activity. *Micro Nano Lett.* **9**, 932–934 (2014). <https://doi.org/10.1049/mnl.2014.0238>
28. B.S. Avinash, V.S. Chathurmukha, C.S. Naveen, M.P. Rajeeva, H.S. Jayanna, A.R. Lamani, Influence of particle size on band gap and dielectric properties of TiO_2 nanomaterials, in: *AIP Conf. Proc.* (A.I.P. Publishing LLC, 2016), p. 20347. <https://doi.org/10.1063/1.4946398>
29. V.M. Kalygina, I.S. Egorova, I.A. Prudaev, O.P. Tolbanov, V.V. Atuchin, Conduction mechanism of metal- TiO_2 -Si structures. *Chinese J. Phys.* **55**, 59–63 (2017). <https://doi.org/10.1016/J.CJPH.2016.08.011>
30. D.V. Gritsenko, S.S. Shaimeev, V.V. Atuchin, T.I. Grigor'eva, L.D. Pokrovskii, O.P. Pchelyakov, V.A. Gritsenko, A.L. Aseev, V.G. Lifshits, Two-band conduction in TiO_2 . *Phys. Solid State* **48**, 224–228 (2006). <https://doi.org/10.1134/S1063783406020053>
31. V.M. Kalygina, I.S. Egorova, I.A. Prudaev, O.P. Tolbanov, V.V. Atuchin, Photoelectrical characteristics of TiO_2 -N-SI heterostructures, microw. Opt. Technol. Lett. **58**, 1113–1116 (2016). <https://doi.org/10.1002/mop.29737>
32. B.H. Toby, Expgui, EXPGUI, a graphical user interface for GSAS. *J. Appl. Cryst.* **34**, 210–213 (2001). https://ncnr.nist.gov/programs/crystallography/software/EXPGUI_reprint.pdf. Accessed 7 Feb 2018
33. A.C. Larson, R.B. Von Dreele, LAUR 86–748 © GENERAL STRUCTURE ANALYSIS SYSTEM, LAUR, (2004). <http://11bm.Xray.aps.anl.gov/documents/GSASManual.pdf>. Accessed 7 Feb 2018
34. M.I. Ahmad, D.G. Van Campen, J.D. Fields, J. Yu, V.L. Pool, P.A. Parilla, D.S. Ginley, M.F.A.M. Van Hest, M.F. Toney, Rapid thermal processing chamber for *in-situ* X-ray diffraction. *Rev. Sci. Instrum.* **86**, 13902 (2015). <https://doi.org/10.1063/1.4904848>
35. S. Sivasankaran, M.J. Kishor Kumar, A novel sonochemical synthesis of nano-size silicon nitride and titanium carbide. *Ceram. Int.* **41**, 11301–11305 (2015). <https://doi.org/10.1016/J.CERAMINT.2015.05.087>
36. S. Chowdhury, G.K. Parshtti, R. Balasubramanian, Post-combustion CO_2 capture using mesoporous TiO_2 /graphene oxide nanocomposites. *Chem. Eng. J.* **263**, 374–384 (2015). <https://doi.org/10.1016/J.CEJ.2014.11.037>
37. D.S. Kim, S.Y. Kwak, The hydrothermal synthesis of mesoporous TiO_2 with high crystallinity, thermal stability, large surface area, and enhanced photocatalytic activity. *Appl. Catal. A Gen.* **323**, 110–118 (2007). <https://doi.org/10.1016/j.apcata.2007.02.010>
38. S. Meti, M.R. Rahman, M.I. Ahmad, K.U. Bhat, Chemical free synthesis of graphene oxide in the preparation of reduced graphene oxide-zinc oxide nanocomposite with improved photocatalytic properties. *Appl. Surf. Sci.* **451**, 67–75 (2018). <https://doi.org/10.1016/J.APSUSC.2018.04.138>
39. V. Uvarov, I. Popov, Metrological characterization of X-ray diffraction methods for determination of crystallite size in nano-scale materials. *Mater. Charact.* **58**, 883–891 (2007). <https://doi.org/10.1016/j.matchar.2006.09.002>
40. L.B. McCusker, R.B. Von Dreele, D.E. Cox, D. Louër, P. Scardi, Rietveld refinement guidelines. *J. Appl. Crystallogr.* **32**, 36–50 (1999). <https://doi.org/10.1107/S0021889898009856>
41. L. Xiang, X. Zhao, J. Yin, B. Fan, Well-organized 3D urchin-like hierarchical TiO_2 microspheres with high photocatalytic activity. *J. Mater. Sci.* **47**, 1436–1445 (2012). <https://doi.org/10.1007/s10853-011-5924-7>
42. H.G. Yang, G. Liu, S.Z. Qiao, C.H. Sun, Y.G. Jin, S.C. Smith, J. Zou, H.M. Cheng, G. Qing, M. Lu, Solvothermal synthesis and photoreactivity of anatase TiO nanosheets with dominant {001} facets. *J. Am. Chem. Soc.* **131** (2009) 4078–4083. <https://doi.org/10.1021/ja808790p>
43. Q. Chen, Q. Liu, J. Hubert, W. Huang, K. Baert, G. Wallaert, H. Terryn, M.-P. Delplancke-Ogletree, F. Reniers, Deposition of photocatalytic anatase titanium dioxide films by atmospheric dielectric barrier discharge. *Surf. Coatings Technol.* **310**, 173–179 (2017). <https://doi.org/10.1016/J.SURFCOAT.2016.12.077>
44. V. Swamy, D. Menzies, B.C. Muddle, A. Kuznetsov, L.S. Dubrovinsky, Q. Dai, V. Dmitriev, Nonlinear size dependence of anatase TiO_2 lattice parameters. *Appl. Phys. Lett.* **88**, 243103 (2006). <https://doi.org/10.1063/1.2213956>
45. V.V. Atuchin, V.G. Kesler, G. Meng, Z.S. Lin, The electronic structure of RbTiOPO_4 and the effects of the A-site cation substitution in KTiOPO_4 -family crystals. *J. Phys. Condens. Matter* **24**, 405503 (2012). <https://doi.org/10.1088/0953-8984/24/40/405503>
46. V.V. Atuchin, V.G. Kesler, N.V. Pervukhina, Z. Zhang, Ti 2p and O 1s core levels and chemical bonding in titanium-bearing oxides. *J. Electron Spectros. Relat. Phenomena* **152**, 18–24 (2006). <https://doi.org/10.1016/J.ELSPEC.2006.02.004>
47. V.V. Atuchin, T.A. Gavrilova, J.-C. Grivel, V.G. Kesler, Electronic structure of layered titanate $\text{Nd}_2\text{Ti}_2\text{O}_7$. *Surf. Sci.* **602**, 3095–3099 (2008). <https://doi.org/10.1016/J.SUSC.2008.07.040>
48. C.V. Ramana, V.V. Atuchin, U. Becker, R.C. Ewing, L.I. Isaenko, O.Y. Khyzhun, A.A. Merkulov, L.D. Pokrovsky, A.K. Sinelnichenko, S.A. Zhurkov (2007) Low-energy Ar + ion-beam-induced amorphization and chemical modification of potassium titanyl arsenate (001) crystal surfaces. <https://doi.org/10.1021/JP0671392>
49. A. Maliakal, H. Katz, P.M. Cotts, S. Subramoney, P. Mirau, Inorganic oxide core, polymer shell nanocomposites as a high gate dielectric for flexible electronics application. *J. Am. Chem. Soc.* **127**, 14655–14662 (2005)
50. I. Wypych, M. Bobowska, A. Tracz, S. Opasinska, A. Kadlubowski, J. Krzywania-kaliszewska, P. Grobelny, Wojciechowski, Dielectric properties and characterisation of titanium dioxide obtained by dielectric properties and characterisation of titanium dioxide obtained by different chemistry methods, *J.Nano.Mat.* (2014) 1–9. <https://doi.org/10.1155/2014/124814>
51. N.N. Rabin, S. Ida, M.R. Karim, M.S. Islam, R. Ohtani, M. Nakamura, M. Koinuma, L.F. Lindoy, S. Hayami, Super dielectric materials of two-dimensional TiO_2 or $\text{Ca}_2\text{Nb}_3\text{O}_{10}$ nanosheet hybrids with reduced graphene oxide. *ACS Omega* **3**, 2074–2083 (2018). <https://doi.org/10.1021/acsomega.7b01764>
52. D. Singh, P. Yadav, N. Singh, C. Kant, M. Kumar, S.D. Sharma, K.K. Saini, Dielectric properties of Fe-doped TiO_2 nanoparticles synthesised by sol–gel route. *J. Exp. Nanosci.* **8**, 171–183 (2013). <https://doi.org/10.1080/17458080.2011.564215>
53. S. Sagadevan, Synthesis and electrical properties of TiO_2 nanoparticles using a wet chemical technique. *Am. J. Nanosci. Nanotechnol.* **1**, 27–30 (2013). <https://doi.org/10.11648/j.nano.20130101.16>
54. A. Tripathy, P. Sharma, N. Sahoo, Synthesis, morphological, electromechanical characterization of $(\text{CaMgFe}_{1-x}\text{Ti}_{x})_{12-\delta}\text{O}_{32}$ PDMS nanocomposite thin films for energy storage application. *IOP Conf. Ser. Mater. Sci. Eng.* **323**, 1–6 (2018). <https://doi.org/10.1088/1745-899X/323/1/012018>
55. T. Paraffin, C. Shell, B. Balasubramanian, K.L. Kraemer, N.A. Reding, R. Skomski, S. Ducharme, D.J. Sellmyer, Synthesis of

- monodisperse properties. *ACS Nano* **4**, 1893–1900 (2010). <https://doi.org/10.1021/nn9016422>
56. V.V. Brus, A.K.K. Kyaw, P.D. Maryanchuk, J. Zhang, Quantifying interface states and bulk defects in high-efficiency solution-processed small-molecule solar cells by impedance and capacitance characteristics. *Prog. Photovolt. Res. Appl.* **23**, 1526–1535 (2015). <https://doi.org/10.1002/pip.2586>

Publisher's Note Springer Nature remains neutral with regard to jurisdictional claims in published maps and institutional affiliations.